PHILOSOPHICAL TRANSACTIONS OF THE ROYAL SOCIETY A MATHEMATICAL, PHYSICAL & ENGINEERING SCIENCES

On the Dynamics of Wind-Driven Shelf Currents

J. S. Allen and R. L. Smith

Phil. Trans. R. Soc. Lond. A 1981 **302**, 617-634
doi: 10.1098/rsta.1981.0187

Phil. Trans. R. Soc. Lond. A **302**, 617–634 (1981)
Printed in Great Britain

On the dynamics of wind-driven shelf currents

By J. S. Allen and R. L. Smith
School of Oceanography, Oregon State University, Corvallis, Oregon 97331, *U.S.A.*

Measurements of currents, wind, and coastal sea level from off Oregon, northwest Africa and Peru are used to examine characteristics of the depth-integrated momentum balance at mid-shelf locations. Attention is focused on determining the nature of the balance, as a function of frequency, of time-dependent terms in the alongshore momentum equation. Decomposition of the estimated terms into empirical orthogonal functions, and regression of terms on the wind stress to obtain the wind-forced component, are methods used in an attempt to assess objectively the type of balance present. It is found, for Oregon, that there is a relatively large amount of variance in the depth-integrated cross-shelf velocity which is not balanced by other estimated terms. In addition, a substantial component of the flow is wind-forced, with bottom friction insignificant for periods less than 11 days. For northwest Africa, the motion is strongly wind-driven, with bottom friction playing an important role for periods greater than 6 days and with a quasi-steady response evident for periods longer than 10 days. For Peru, the motion is dominated by an inviscid, unforced balance which, for the 5- to 11-day frequency band, is primarily between the alongshore pressure gradient and the rate of change with time of the alongshore velocity.

1. Introduction

Knowledge of the characteristics of current régimes on continental shelves has increased tremendously over the past ten years as a result of the availability of measurements from moored current meters. Along with the increase of information from current measurements and other observations, many theoretical models have been developed for application to shelf flow fields. Different analytical models have included a variety of simplifying assumptions (Allen 1980). Currently, it is not clear under exactly what conditions, or for what shelf regions, many of these assumptions are valid. Probably the simplest theoretical context in which assumptions on the relative importance of various dynamical processes enter significantly is provided by the depth-integrated momentum equations. In this paper, we use current measurements from three different continental shelves to examine characteristics of the depth-integrated momentum balance and to assess the relative importance of various terms, and hence of various processes, in that balance. We concentrate on motions with time-scales of several days, i.e. with periods greater than inertial or tidal periods, corresponding to the dominant time-scales of the atmospheric forcing.

The observations analysed here were made as part of the Coastal Upwelling Ecosystems Analysis (C.U.E.A.) program in field experiments off Oregon, U.S.A., in July–August 1973, off northwest Africa in March–April 1974, and off Peru in March–May 1977. Although the existence of wind-forced coastal upwelling is a prominent feature of the circulation on all of these shelves, there are substantial qualitative differences in the nature of the flow fields which, as we shall discuss, are associated with different dynamical balances.

In each of the three regions of the C.U.E.A. field experiments, horizontal velocities were

measured in the surface layer from closely spaced current meters on a mooring at a mid-shelf location (see, for example, Halpern 1976*a*). Simultaneously, horizontal velocities were measured in the water column below from less densely spaced instruments on a separate mooring at essentially the same position. The relative locations of these current meters and the cross-shelf bottom topography for Oregon, northwest Africa and Peru are shown in figure 1. These current measurements probably provide the best currently available vertical resolution of continental-shelf velocity fields in water of depth 70–120 m. Consequently, this particular data set is especially appropriate for, among other things, relatively accurate calculations of depth-averaged velocity fields.

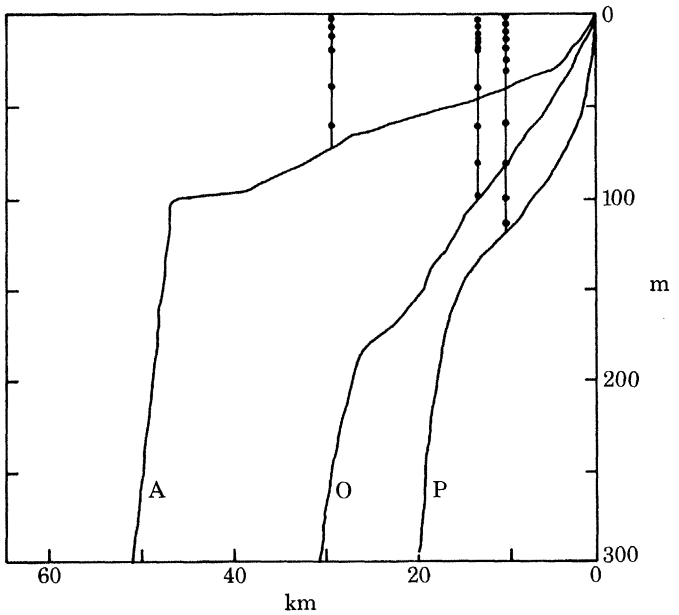

FIGURE 1. Continental shelf and slope topography off northwest Africa (A) (21° 40′ N), Oregon (O) (45° 16′ N) and Peru (P) (15° 06′ S) with the locations of the moored instrument arrays shown.

The basic characteristics of the shelf flow fields off Oregon, northwest Africa and Peru during the C.U.E.A. field experiments have been described in previous publications. A brief summary of some of the major features, and several references are given below. An especially pertinent reference is Smith (1981), in which the spatial structure, time variability, and mass balance of the flow fields in the three upwelling regions are compared by using the same measurements that are further analysed here. Some aspects of the depth-integrated momentum balances have been examined for Oregon by Allen & Kundu (1978), for Peru by Brink & Allen (typescript in preparation), and for northwest Africa by Badan-Dangon (1981). Those studies are extended in this paper.

On the Oregon shelf, the stratification is strong (a difference of 2 σ_t units between the surface and bottom). At mid-shelf, the mean flow is baroclinic (equatorward and offshore in a surface layer 20 m deep, equatorward and strongly onshore at mid-depth, and poleward near the bottom), but the subtidal fluctuations in the alongshore component of the flow are nearly barotropic and tend to align along the local isobaths. Throughout the water column the alongshore velocity fluctuations are significantly correlated with the local wind stress, which has a standard deviation greater than the mean (Smith 1974; Kundu & Allen 1976; Allen & Kundu 1978).

For northwest Africa, the stratification over the wide shallow shelf is weaker than off Oregon (a difference of 0.3 σ_t units between surface and bottom), the mean vertical shear of the alongshore velocity is less at mid-depth but greater near the bottom, the layer of offshore flow is deeper (35 m), and the strongest onshore flow occurs within 10 m of the bottom. The velocity fluctuations are significantly correlated with the wind stress, which has a standard deviation only slightly larger than it has off Oregon but a mean value three times larger (Huyer 1976; Halpern *et al.* 1977).

Off Peru, the stratification is less than half that off Oregon but both the mean and fluctuating flow exhibit substantial shear associated with baroclinic effects. Except in an Ekman surface layer of about 25 m thickness where the mean flow is equatorward and offshore, the mean alongshore velocities are poleward and counter to the persistently equatorward trade wind. The strongest onshore flow is above mid-depth, and weak mean offshore flow occurs within about 10 m of the bottom. The mean wind stress is greater than that off Oregon, but the standard deviation is about half. Although the cross-shelf component of the velocity is correlated with the wind stress, the larger alongshore component is not. The 5- 10-day-period fluctuations in the alongshore current propagate poleward at about 200 km day^{-1} (Smith 1978; Brink *et al.* 1980).

2. Depth-integrated equations

A right-handed Cartesian coordinate system (x, y, z) is used with the y-axis alongshore, the x-axis across the shelf, and the z-axis vertical; x is positive onshore. The corresponding velocity components are (u, v, w). The surface is assumed to be a rigid lid at $z = 0$ while the bottom is at $z = -H(x, y)$.

On the subinertial time-scales of primary interest here, order-of-magnitude arguments based on the assumption $v \gg u$ indicate that the depth-integrated cross-shelf momentum equation should be dominated by the geostrophic balance of the alongshore velocity v. This is also a common approximation in theoretical models, where other assumptions affect primarily the balances in the y-momentum equation. All of the observations from the regions under study are consistent with assumptions of geostrophic balance for v (as are results from analyses of terms in the x-momentum equation similar to those applied to the y-momentum equation in §§3 and 4). Consequently, we focus our attention here on the alongshore momentum balance.

The depth-integrated continuity and y momentum equations are

$$U_x + V_y = 0, \tag{1}$$

$$V_t + N^v + fU = -P_y + \tau_W - \tau_B, \tag{2}$$

where

$$(U, V, \tilde{P}) = \int_{-H}^{0} (u, v, p)\, dz, \tag{3}$$

$$N^v = \left(\int_{-H}^{0} uv\, dz\right)_x + \left(\int_{-H}^{0} v^2\, dz\right)_y, \tag{4}$$

$$P_y = \tilde{P}_y - p_B H_y, \quad p_B = p(z = -H). \tag{5}$$

Here p is the pressure, τ_W and τ_B the wind and bottom stress components in the y-direction (all divided by a reference density), t is time and f the Coriolis parameter. Subscripts (x, y, t) denote partial differentiation. Stress terms due to horizontal turbulent diffusion are neglected.

Common approximate balances in the alongshore momentum equation (2), which might be observed in the data, are as follows.

Linear. The nonlinear term N^y is neglected on the argument that the Rossby number $\epsilon = V_0(f\delta_x)^{-1}$ is reasonably small, where V_0 is a characteristic alongshore velocity and δ_x a characteristic cross-shelf scale, for example, with $V_0 = 20$ cm s^{-1}, $\delta_x = 20$ km, $f = 10^{-4}$ s^{-1}, $\epsilon = 0.1$. The resulting equation is

$$V_t + fU = -P_y + \tau_W - \tau_B. \tag{6}$$

Subsequent assumptions will be discussed within the linear approximation.

Two-dimensional. In purely two-dimensional flow, where the derivative of all variables with respect to y equals zero, it follows that $fU = 0$, $P_y = 0$ and

$$V_t = \tau_W - \tau_B. \tag{7}$$

Quasisteady. In quasisteady, or steady, flow the time-derivative V_t is neglected as being small relative to other terms:

$$fU = -P_y + \tau_W - \tau_B. \tag{8}$$

For a barotropic fluid, with a linear relation between bottom stress and alongshore velocity, this leads to the 'arrested topographic wave' solutions (Csanady 1978). The application of this type of approximation in shallow shelf waters is discussed by Csanady (this symposium).

Frictionless. In this case $\tau_B = 0$ and

$$V_t + fU = -P_y + \tau_W. \tag{9}$$

Free and frictionless. The wind stress $\tau_W = 0$ and $\tau_B = 0$. Because of the waveguide nature of continental margins (see, for example, Allen 1980) the motion is usually thought of as composed of free coastal trapped waves:

$$V_t + fU = -P_y. \tag{10}$$

If in (10) $\tau_B \neq 0$, the motion is free and frictionally damped.

Two-dimensional, quasisteady, frictionless. These conditions could conceivably apply for large alongshore scale, low frequency, stratified motion (Enfield & Allen 1980). Here $fU = 0$, but $P_y \neq 0$ so that

$$0 = -P_y + \tau_W. \tag{11}$$

Equation (11) corresponds to a mass balance for the cross-shelf flow such that offshore (onshore) Ekman transport is compensated by a geostrophic onshore (offshore) velocity beneath the surface layer.

3. Alongshore momentum equation

3.1. *Estimation of Terms*

Current, coastal sea level, and buoy wind measurements are used to evaluate terms in the depth-integrated alongshore momentum equation (2) at the mooring locations shown in figure 1. Details of the observations and of the data processing procedures are given in the Appendix.

Depth-integrated currents were calculated by using the trapezoidal rule. Errors in that calculation are discussed in the Appendix. The orientation of the (x, y) coordinate system is chosen, after Smith (1981), to coincide with the principal axes of the depth-integrated velocity components, i.e. of the mass transport. The resulting 'alongshore' direction is close to that estimated for smoothed isobaths running through the location of the moorings (see Appendix).

The use of the mass transport principal axes seems to be especially appropriate here since, as will be seen from the results, off Oregon and northwest Africa fU has a larger variance than can be accounted for by balances with other evaluated terms. In the mass transport principal axes system, the variance of fU is minimized. Hence there is no excess variance in fU caused by the alignment of the coordinate system.

The time-derivative V_t is formed by applying a centred difference approximation to the low-passed time series with $2\Delta t = 12$ h, as in Allen & Kundu (1978). Negligible differences were found between the results of this procedure and that of time-differencing the higher frequency hourly data (see Appendix) with $2\Delta t = 2$ h and then low-pass filtering.

The bottom stress was calculated with the hourly velocity data ($\hat{u}_B$, $\hat{v}_B$) from the bottom current meters (5, 7 and 6 m above the bottom for Oregon, northwest Africa, and Peru, respectively). A quadratic drag law

$$\hat{\tau}_B = C_D(\hat{v}_B^2 + \hat{u}_B^2)^{\frac{1}{2}}\hat{v}_B, \tag{12}$$

with $C_D = 1.5 \times 10^{-3}$ was used and then the resulting hourly time series $\hat{\tau}_B$ was low-pass filtered to give τ_B.

The wind stress τ_W was also calculated by using a quadratic drag law from wind measurements at surface buoys near the locations of the moorings (see Appendix).

The pressure gradient term P_y was approximated for Oregon and Peru by differencing coastal sea level measurements from nearby tide gauges at different alongshore locations:

$$P_y \approx gH_0(\zeta_2 - \zeta_1)/\Delta y, \tag{13}$$

where g is the acceleration due to gravity, H_0 is the total water depth at the mooring, ζ_1, ζ_2 are sea level heights at coastal stations 1 and 2, and Δy is the alongshore distance between stations 1 and 2 ($\Delta y = 104$, 230 km for Oregon, Peru). This approximation for P_y accounts neither for baroclinic contributions to the pressure gradient nor for a possible decay in magnitude of $\zeta_2 - \zeta_1$ across the shelf, from the coast to the mooring site.

The four terms V_t, fU, τ_W and τ_B in (2) may be estimated by using direct measurements from a single location without additional errors from approximations of spatial derivatives. The barotropic contribution to the alongshore pressure gradient term P_y is estimated from coastal sea-level measurements and that does require an approximation for a spatial derivative. The pressure gradient, however, is likely to play such a fundamental role in the alongshore momentum balance that we felt it was desirable to include approximation (13) when the sea-level data were available.

Estimations of the nonlinear terms N^y (equation (4)) require spatial derivatives of depth-integrated momentum fluxes. Since an equivalent set of current measurements generally did not exist from adjacent moorings, difference approximations for the terms in N^y could not be formed from measured variables. Consequently, we did not attempt to estimate N^y.

The nonlinear momentum flux terms (4) and the baroclinic contribution to the pressure gradient are thus two possible contributors to the balance in (2) that are not represented in the subsequent analysis.

3.2. *Observations*

The mean values and standard deviations of the estimated terms in (2) from Oregon, northwest Africa, and Peru are given in table 1 and are denoted by overbars and primes, respectively. Since absolute sea-level elevations are not known, the mean values of P_y cannot be

calculated. We concentrate on assessing the possible balance of the time-dependent fluctuations of the estimated terms. The time series are plotted in figures 2, 3 and 4, and the cross-correlation matrices of these terms are given in table 2.

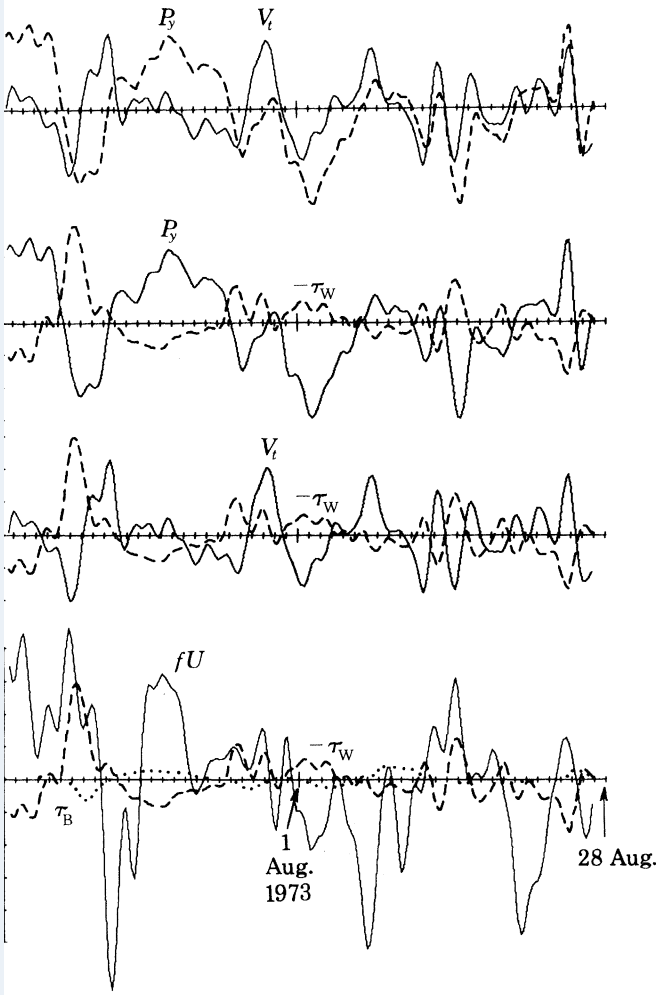

2. Time series of V_t, fU, P_y, τ_B and τ_W (with mean values removed) for Oregon.

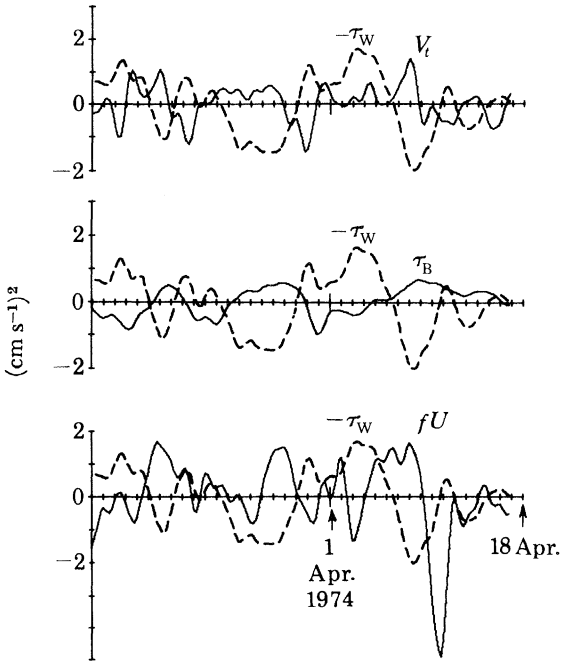

FIGURE 3. Time series of V_t, fU, τ_B and τ_W (with mean values removed) for northwest Africa.

We are also interested in the frequency dependence of the balance in (2), which we investigate by band-pass filtering the time series into three frequency bands corresponding to periods of (i) greater than 10 days, (ii) 5–11 days, and (iii) 2–6 days. Autospectra for the estimated terms are plotted in figure 5, and the standard deviations of the original series and of the band-passed series are plotted in figure 6.

For Oregon, the positive correlation of the pairs of variables (V_t, τ_W), (P_y, τ_W), and (V_t, P_y) is apparent in figure 2 (see also table 2). The fact that the correlations are positive is consistent with wind-stress-forcing of V_t and P_y, as in (7) and (11) for simpler cases. The positive correlation between V_t and P_y is compatible with both these variables being forced by τ_W, but not with V_t, P_y balance in (10). The bottom stress τ_B is also positively correlated with τ_W and P_y, again consistent with a response of both τ_B and P_y to wind stress.

PHILOSOPHICAL TRANSACTIONS OF THE ROYAL SOCIETY A MATHEMATICAL, PHYSICAL & ENGINEERING SCIENCES

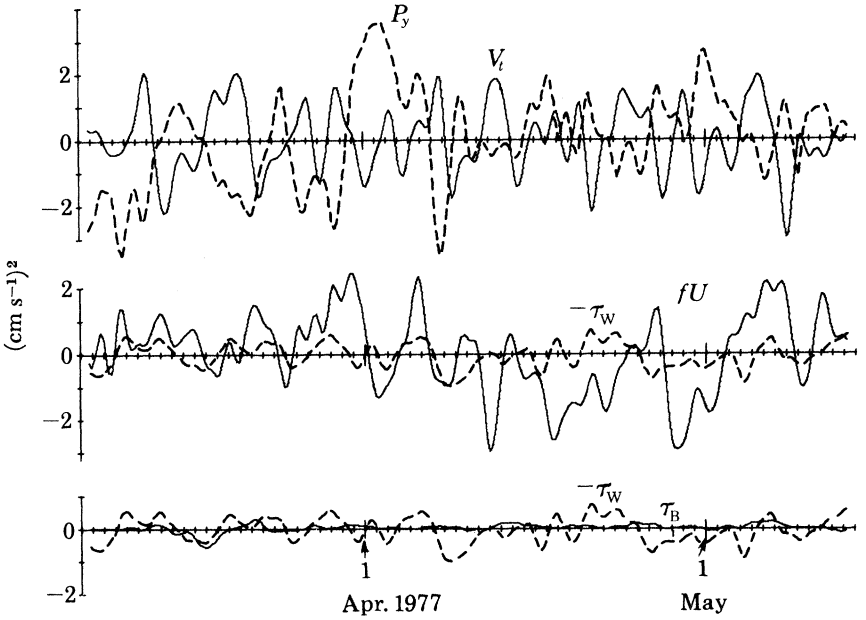

FIGURE 4. Time series of V_t, fU, P_y, τ_B and τ_W (with mean values removed) for Peru.

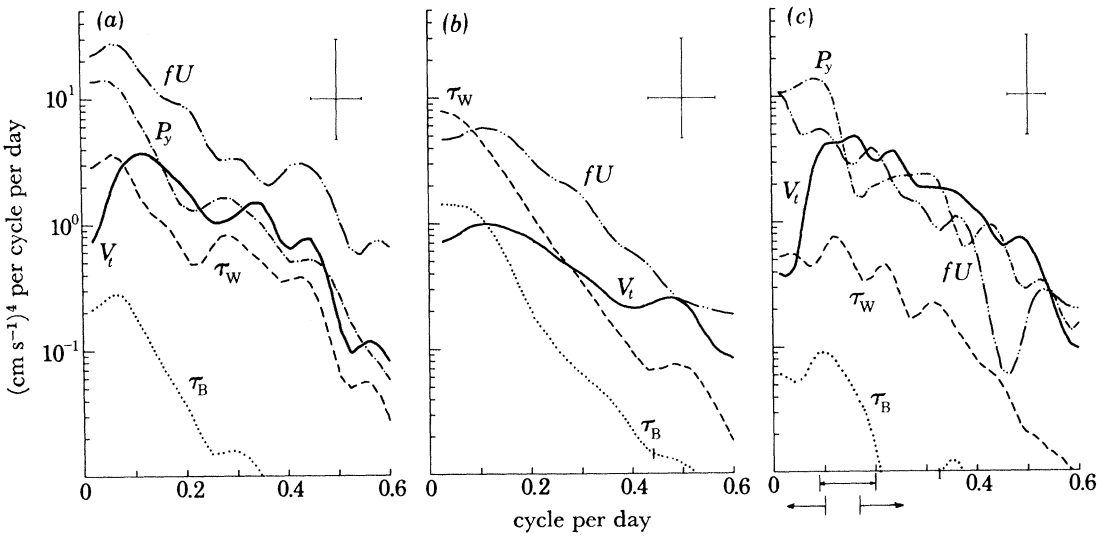

FIGURE 5. Autospectra of V_t, fU, P_y, τ_B and τ_W for (*a*) Oregon, (*b*) northwest Africa, and (*c*) Peru (P_y is absent for northwest Africa). The 95% confidence limit and the equivalent statistical bandwidth for the spectral estimates are shown in the upper right-hand corners. Frequency bands (less than 0.1, 0.09–0.2, 0.17–0.6 cycle per day (half power points)) corresponding to periods of greater than 10, 5–11, and 2–6 days, used for the band-pass filtered series, are indicated on the frequency axis of (*c*).

For all frequency bands, fU has the largest magnitude, but it is not significantly correlated with any of the other variables. Smith (1981) examined the time-dependent behaviour of the depth-integrals of the cross-shelf velocity over the surface layer H_S and over the interior. Off Oregon (H_S = 20 m), it was found that the surface layer integral fU_S is well correlated with τ_W and that the sign and magnitude of the regression coefficient of fU_S on τ_W are in agreement with those expected for Ekman transport. The interior depth-integral fU_L has a correlation with τ_W opposite in sign and lower in magnitude than that between fU_S and τ_W, while fU_L

and fU_S are not well correlated. Thus, the surface and interior cross-shelf transports show some consistency with a wind-forced model, but the surface layer flow is much more tightly coupled to τ_W than is the interior flow. Similar results were found off northwest Africa and Peru (H_S = 35, 32 m, respectively). Here we find, however, that the total depth-integrated fU off Oregon has a time-dependent behaviour and a magnitude that are not clearly related to the other estimated terms in the alongshore momentum balance (2).

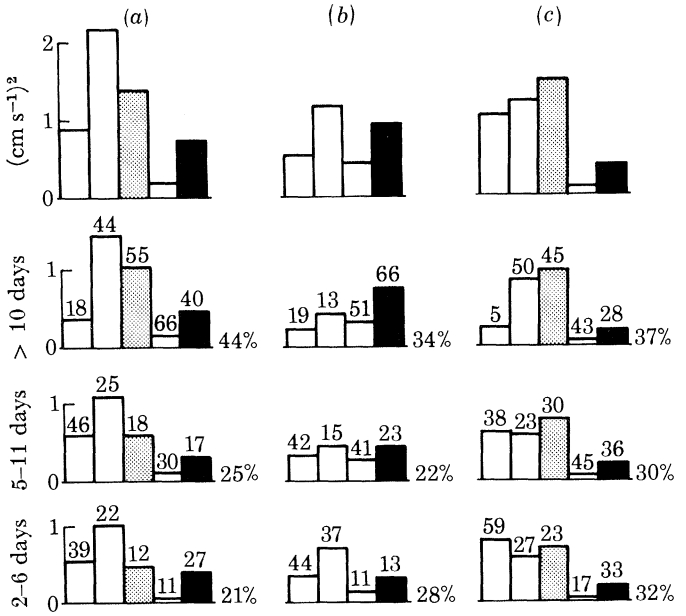

FIGURE 6. Standard deviations of V_t, fU, P_y, τ_B, and τ_W from (*a*) Oregon, (*b*) northwest Africa, and (*c*) Peru for the original and for the band-passed time series. For each case, the standard deviations are plotted from left to right in the order V_t, fU, P_y (stippled), τ_B, and τ_W (solid black) except for northwest Africa where P_y is absent. The total *variance* (sum of the variances of each term) in each frequency band, expressed as a percentage of the total variance of the original series, is given to the right of the plots. The *variance* of individual terms in each frequency band, expressed as a percentage of the variance of that term in the original series, is indicated directly over the plotted values.

TABLE 1. MEANS AND STANDARD DEVIATIONS

term	Oregon		northwest Africa		Peru	
$(\text{cm s}^{-1})^2$	mean	s.d.	mean	s.d.	mean	s.d.
V_t	—	0.89	—	0.54	—	1.05
fU	1.34	2.18	0.48	1.17	−0.60	1.22
P_y	—	1.39	—	—	—	1.47
τ_W	−0.51	0.74	−1.50	0.95	0.79	0.40
τ_B	0.05	0.18	−0.53	0.44	−0.05	0.12

The amplitudes of V_t and P_y off Oregon (figure 5) are similar for periods less than 10 days, while τ_W is slightly smaller and τ_B substantially smaller. For periods greater than 10 days, the amplitude of V_t decreases with increasing period, but it still remains larger than that of the bottom stress τ_B for all the resolved frequency bands. The ratio of τ'_B to V'_t is largest for periods greater than 10 days and smallest for periods less than 6 days.

For northwest Africa, the positive correlations of the pairs (V_t, τ_W) and (τ_B, τ_W) is clear from figure 3, as is the weakness of the correlation of fU with the other variables. The wind stress

τ_W and fU generally have the largest amplitudes, with $\tau'_W > fU'$ for periods greater than 10 days and $fU' > \tau'_W$ for periods less than 6 days. In contrast to Oregon, τ'_B is greater than V'_t for periods greater than 10 days while it is comparable with V'_t for periods of 5–11 days and less than V'_t for periods of 2–6 days.

For Peru, the negative correlation of V_t and P_y, obvious in figure 4, is consistent with a V_t, P_y balance in (10). The amplitudes of P_y, fU, and V_t (figure 5) are generally comparable except for periods greater than 10 days where V_t is smaller. Unlike both Oregon and northwest Africa, the wind stress is substantially smaller than fU and P_y for all frequency bands and is smaller than V_t for periods less than 10 days. The amplitude of the bottom stress τ_B is less than that of any other term.

TABLE 2. CROSS-CORRELATION COEFFICIENTS

	Oregon				northwest Africa			Peru			
	fU	P_y	τ_B	τ_W	fU	τ_B	τ_W	fU	P_y	τ_B	τ_W
V_t	−0.26	0.31†	0.06	0.45†	0.29	−0.04	0.34†	−0.10	−0.40†	0.13	−0.02
fU	—	0.19	−0.05	−0.09	—	0.06	0.20	—	−0.19	0.18	−0.21
P_y	—	—	0.57†	0.68†	—	—	—	—	—	−0.13	0.11
τ_B	—	—	—	0.57†	—	—	0.70†	—	—	—	−0.14

† The probability that this correlation coefficient would be obtained from uncorrelated variables is less than 0.1.

TABLE 3. CROSS-CORRELATION COEFFICIENTS, REGRESSION COEFFICIENTS, STANDARD DEVIATIONS, APPROXIMATE RESISTANCE COEFFICIENTS, AND SPIN-DOWN TIMES

	$\{\tau_B, v_B\}$	$r_R \pm$ standard error, 10^{-2} cm s^{-1}	v'_B, cm s^{-2}	V', 10^4 cm^2 s^{-2}	$C_D(\overline{\hat{u}_B^2+\hat{v}_B^2})^{\frac{1}{2}}$, 10^{-2} cm s^{-1}	$V'/r_R v'_B$, day
Oregon	0.97†	2.02 ± 0.12	8.66	10.14	1.40	6.7
northwest Africa	0.96†	4.45 ± 0.40	9.46	6.58	2.79	1.8
Peru	0.94†	2.04 ± 0.14	5.51	11.49	1.25	11.8

† The probability that this correlation coefficient would be obtained from uncorrelated variables is less than 0.01.

In the above discussion, the possible balance of four or five terms is assessed by referring to cross-correlation matrices and standard deviations. This is clearly not as systematic a procedure as might be desired. In the following section, we propose and apply a more objective method for the evaluation of mutual balances.

Before proceeding, we mention a secondary result of interest. Based on a comparison with the nonlinear bottom stress computed by (12), the linear approximation commonly used in analytical models, $\tau_{BL} \approx r v_B$, where r is a resistance coefficient and v_B is a low-passed bottom velocity, appears to be reasonably good. The correlation coefficients between τ_B and v_B denoted by curly brackets $\{\tau_B, v_B\}$, and the regression coefficients r_R from the regression of τ_B on v_B are given in table 3. The correlations are all very high. The regression coefficients r_R provide estimates for r. We note (see table 3) that these are higher by factors of 1.4 to 1.6 than approximate values given by $r \approx C_D(\overline{\hat{u}_B^2+\hat{v}_B^2})^{\frac{1}{2}}$. The implied spin-down times $T_F = V'(r_R v'_B)^{-1}$ are 6.7, 1.8, and 11.8 days for Oregon, northwest Africa, and Peru, respectively. Since periods $T = 2\pi/\omega$ for which a quasisteady-state solution would exist in an equation like $V_t + T_F^{-1}V = \tau_{W0} \exp(i\omega t)$ are $T \gg 2\pi T_F$, these values of T_F are consistent with the relative amplitudes of V_t and τ_B in the autospectra (figure 5).

4. Balance of terms

To estimate the extent and type of mutual balance of time-dependent terms in an equation such as (2), we propose the decomposition of those terms into empirical orthogonal functions. In oceanography these functions have been commonly used in data analysis to represent compactly a large set of observations of a particular variable that is a function of space and time (see, for example, Kundu *et al.* 1975; Davis 1976).

The application here is as follows. Suppose we have N terms $g_i(t)$, $i = 1, \ldots, N$, that are functions of time. Assume the mean values of the terms have been removed, i.e. $\bar{g}_i = 0$, where the overbar denotes a time mean. These terms can be written (see, for example, Kundu *et al.* 1975; Davis 1976) as a sum of N time series

$$g_i(t) = \sum_{n=1}^{N} E_n(t)\, \phi_i^n, \tag{14}$$

where ϕ_i^n is the ith component of the nth eigenvector of the covariance matrix $\overline{g_i\, g_j}$. The eigenvectors are orthogonal; they are normalized so that $\Sigma_{i=1}^{N} \phi_i^n \phi_i^m = \delta_{nm}$ and are ordered so that the eigenvalues $\lambda_n \gg \lambda_{n+1}$.

Results of the decomposition and properties of empirical orthogonal functions that make them appear useful for evaluating balances of terms are

(i) the amplitudes $E_n(t)$ represent a common time dependence for all terms;

(ii) each empirical eigenfunction, taken in order, extracts the maximum amount of total variance possible with a representation such as (14), i.e. with $\hat{g}_i = \Sigma_{n=1}^{M} E_n\, \phi_i^n$, $M < N$, the mean square error $\Sigma_{i=1}^{N} \overline{(g_i - \hat{g}_i)^2}$ is minimized (see, for example, Davis 1976);

(iii) the $E_n(t)$ are uncorrelated, i.e. $\overline{E_n\, E_m} = \delta_{nm}\, \lambda_n$.

Terms, or component parts of terms, may balance each other when they have the same time dependence, such as represented by $E_n(t)$ in (14). For an exact balance with a particular n, the sum of the eigenvector components would equal zero: $\Sigma_{i=1}^{N} \phi_i^n = 0$. An exact balance should not necessarily be expected here, however, since there are potentially important contributions to (2), such as P_y off northwest Africa and the baroclinic part of P_y off Oregon and Peru, that have not been included. The extraction of the maximum amount of the total variance from all terms appears to be a reasonable condition for determining a common time variability. The fact that the $E_n(t)$ are uncorrelated suggests that the different modes may be able to represent separate physical processes in (2), such as locally forced motion and free coastal trapped waves (see, however, §6).

By using the estimated terms $V_t, fU, P_y, \tau_B, -\tau_W$ from each region (with signs as if all terms were on the left-hand side of (2)), empirical orthogonal functions were calculated for the original and for the band-passed time series. The eigenfunctions for the first two modes are shown in figures 7, 8 and 9, where the magnitudes of the ϕ_i^n are plotted. The sum

$$R = -\sum_{i=1}^{N} \phi_i^n, \tag{15}$$

is also shown, since this is the relative magnitude that the sum of the unrepresented terms and the errors would have for an exact balance. The percentage of the total variance accounted for by each mode is listed, as is the percentage of the variance of each variable represented in that particular mode.

PHILOSOPHICAL TRANSACTIONS OF THE ROYAL SOCIETY A MATHEMATICAL, PHYSICAL & ENGINEERING SCIENCES

The main results are the following. Off Oregon (figure 7), the first mode for the original series and for all three frequency bands is dominated by fU. Since the amplitude of R is relatively large, fU is not balanced by other estimated terms. It is not clear exactly what other processes balance fU, but because the fluctuating u-velocities below the surface layer have substantial vertical shear while the fluctuating v-components do not (Kundu & Allen 1976), the baroclinic contribution to P_y is one obvious candidate.

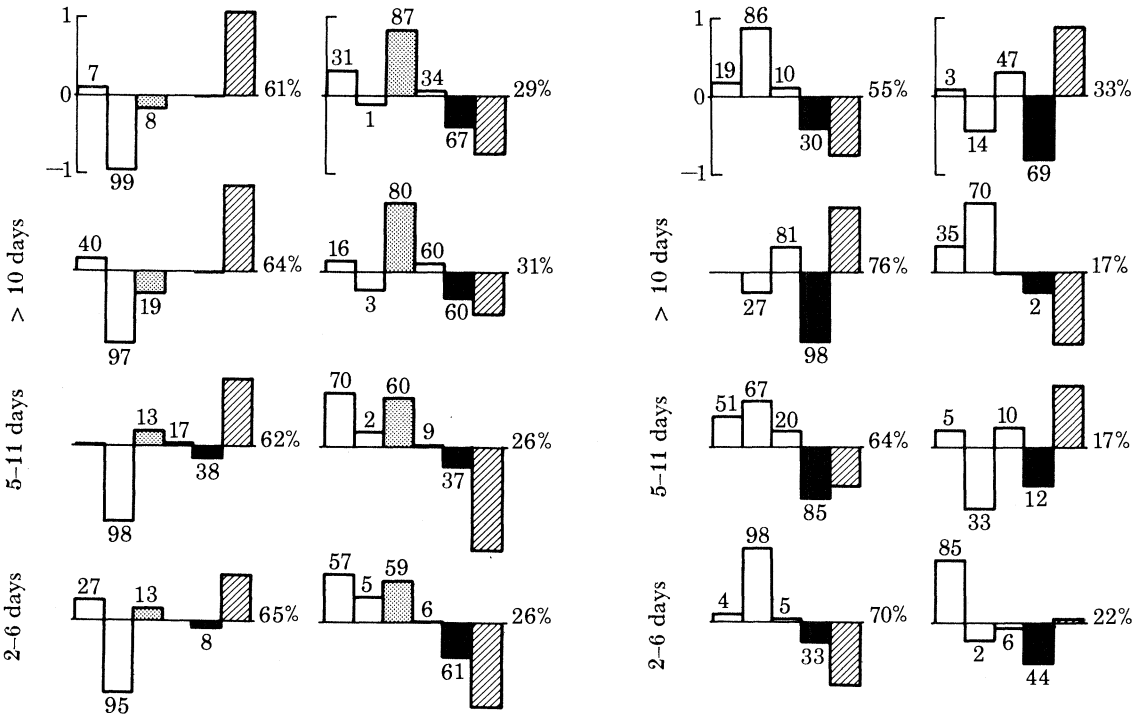

FIGURE 7. The components ϕ_i^n of the first two ($n = 1, 2$) eigenfunctions for $V_t, fU, P_y, \tau_B, -\tau_W$ from Oregon for the original and for the band-passed time series. The components are plotted from left to right in the order V_t, fU, P_y (stippled), τ_B, and τ_W (solid black). To the right of τ_W, the value of $R = -\Sigma_{i=1}^{5} \phi_i^n$ (see equation (15)) is plotted (diagonal shading). The first ($n = 1$) eigenfunctions are in the left-hand column and the second ($n = 2$) eigenfunctions are in the right-hand column. The percentage of the total variance explained by each eigenfunction is given to the right of the plots. The percentage of the variance of each term represented in that eigenfunction is indicated directly above or below the plotted value of ϕ_i^n for that term.

FIGURE 8. The components ϕ_i^n of the first two eigenfunctions for $V_t, fU, \tau_B, -\tau_W$ from northwest Africa for the original and for the band-passed time series. The plots and numbers are as in figure 7 except that P_y is absent, which makes the order of components from left to right V_t, fU, τ_B, τ_W (solid black), and R (diagonal shading).

The second mode for Oregon appears to represent the wind-driven component of the flow. The relative signs of the ϕ_i^n are consistent with V_t, P_y and τ_B being forced by τ_W. The magnitude of τ_W is not large enough, however, to account for the total magnitude of the other terms. The variability in those terms may be related to a non-local response to the wind stress where fluctuations, forced at other locations by a large-scale, coherent wind stress, propagate alongshore as coastal trapped waves. For periods greater than 10 days, P_y is substantially larger than V_t and it appears to dominate the response to τ_W as in (11), while V_t and τ_B are of approximately the same magnitude. This may indicate that the apparent quasisteady response of the alongshore velocity v to τ_W on these time-scales (see, for example, Kundu *et al.* 1975) is the result of an

inviscid adjustment through coastal trapped wave propagation (see, for example, Allen 1980), rather than a result of frictional effects. In the 5–11 and 2–6 day bands, V_t and P_y have a similar magnitude, with τ_B much smaller than both.

Off northwest Africa (figure 8), for periods greater than 10 days, the first mode represents most of the wind stress variance, which is balanced by τ_B and R. If R corresponds to a pressure

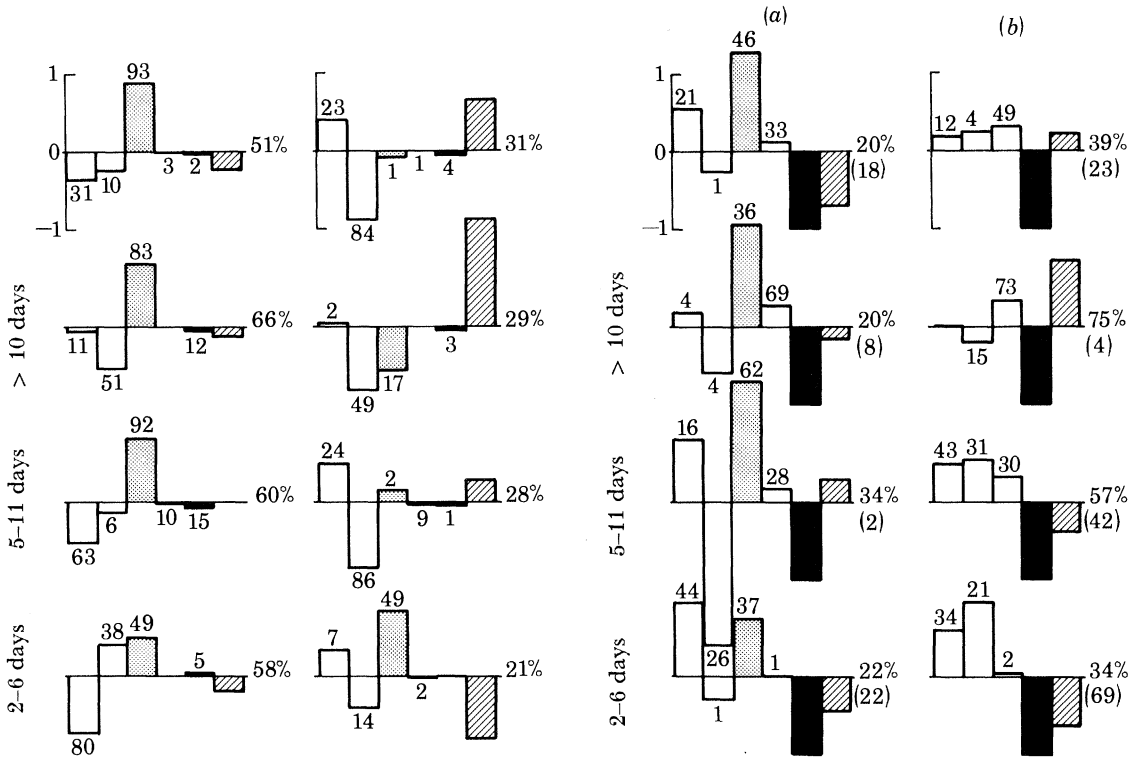

FIGURE 9. The components ϕ_i^n of the first two eigenfunctions for $V_t, fU, P_y, \tau_B, -\tau_W$ from Peru for the original and for the band-passed time series. The plots and numbers are as in figure 7.

FIGURE 10. The regression coefficients b_i from the regression of V_t, fU, P_y, τ_B on τ_W for the original and for the band-passed time series from (*a*) Oregon and (*b*) northwest Africa. The coefficients are plotted from left to right in the order V_t, fU, P_y (stippled, absent for northwest Africa), τ_B, followed by the relative amplitude (-1) of $-\tau_W$ (solid black) and by $R_r = 1 - \Sigma_{i=1}^{N} b_i$ (see equation (16)). The percentage of the total variance explained by τ_W (10^2F) is given to the right of the plots. The percentage of the variance of the sum of terms accounted for by τ_W is given in parentheses below 10^2F. For each term, the percentage of the variance explained by τ_W is given directly above or below the plotted value of b_i for that term. The standard errors of the regression coefficients are given in table 4.

gradient, its sign is consistent with (11). The magnitude of V_t is negligible and this clearly signifies a quasisteady balance as in (8). In the 5- to 11-day band, the first mode again carries most of the wind stress variance. In it, V_t, fU, and τ_B all have signs consistent with a response to forcing by τ_W but, as found off Oregon, the magnitude of τ_W is not large enough to account for all of the variability in these terms. Since V_t is about twice as large as τ_B, the motion is basically time-dependent, but with bottom friction playing an appreciable role. The sign of the cross-shelf transport fU is the same as that expected for the surface Ekman layer flux and hence the cross-shelf flow might be termed upper-layer dominated. In the 2- to 6-day band, the wind stress variance is present in both the first and second modes. The first mode appears to represent

an upper-layer-dominated response of fU to τ_W, but where again τ_W is not large enough to account for all of fU. The second mode, on the other hand, indicates a forcing of V_t by τ_W.

Off Peru (figure 9), the first mode represents a balance of V_t, fU, and P_y, as in example (10), for all frequency bands. The wind stress and bottom stress do not enter appreciably and R is very small. For periods greater than 10 days, V_t is small and fU balances P_y. In the 5- to 11-day band, V_t essentially balances P_y. This is the frequency band in which the fluctuations in v and sea level have been found to propagate poleward (Smith 1978). The momentum balance indicated here is consistent with free coastal trapped waves where, based on the dominance of V_t and P_y over fU, dynamics similar to that of internal Kelvin waves are indicated. In the 2- to 6-day band, fU plays a relatively larger role with its sign opposite to that of V_t. The second mode also indicates an inviscid motion, but with different combinations of V_t, fU, and P_y.

5. Wind-forced component

Another method for examining the momentum balance (2) is to treat the wind stress τ_W as a forcing function and to determine the response of the other variables to τ_W. This procedure may be contrasted with that in §4, where all estimated terms in (2) are considered equally. Here the response to τ_W is called the wind-forced component of the flow. We define the wind-forced component to be the part of each term correlated at zero lag with the wind stress, which is found by linear regression of that term on τ_W. The regression coefficients then provide relative magnitudes of the terms with a common time dependence given by τ_W.

The regression coefficient of a term g_i on τ_W, with $\bar{g}_i = \bar{\tau}_W = 0$, is $b_i = \overline{g_i \tau_W}/\overline{\tau_W^2}$ and the wind-forced component of g_i is $\hat{g}_i = b_i \tau_W$. The regression coefficient b_T of the sum of N terms, $G = \Sigma_{i=1}^N g_i$, is the sum of the individual coefficients, i.e. $b_T = \Sigma_{i=1}^N b_i$. The fraction of the variance of g_i explained by τ_W is given by $\{g_i, \tau_W\}^2$ and likewise the fraction of the variance of G explained by τ_W is $\{G, \tau_W\}^2$, where $\{\ldots\}$ denotes correlation coefficient. The fraction of the total variance accounted for by regression on τ_W is $F = (\Sigma_{i=1}^N \overline{\hat{g}_i^2} + \overline{\tau_W^2})/(\Sigma_{i=1}^N \overline{g_i^2} + \overline{\tau_W^2})$, where $10^2 F$ is analogous to the percentage variance explained by a single empirical orthogonal mode in §4.

The coefficients b_i from the regression of each estimated term V_t, fU, P_y, τ_B on τ_W were calculated for the original and for the band-passed time series. The regression coefficients for Oregon and northwest Africa are given in table 4 and plotted in figure 10. For comparison with the results of §4, the relative amplitude of τ_W, as if it were on the left-hand side of (2), i.e. -1, and the additional amplitude required for an exact balance

$$R_r = 1 - \sum_{i=1}^{N} b_i, \tag{16}$$

are also plotted in figure 10. In addition, the percentage of the variance explained by the wind stress for the sum of terms G and for each individual term is listed as is the percentage of the total variance explained ($10^2 F$). The results for Peru are not shown since there the wind stress does not account for an appreciable amount of the total variance (for example, $F = 0.05$ for the original time series).

For Oregon, the distribution of regression coefficients is similar to the relative magnitudes obtained for the second mode from the empirical orthogonal function (e.o.f.) analysis (figure 7). In both, the signs of V_t, P_y, and τ_B relative to $-\tau_W$ are the same for all frequency bands, and the

relative magnitudes are qualitatively similar, except in the 5- to 11-day band. The sign of R_r is the same as that of $-\tau_W$, except again in the 5- to 11-day band, indicating that the magnitude of τ_W is not large enough to balance the other terms, as was found from the second mode of the e.o.f. analysis. The terms in the regression analysis are evidently closer to a balance, however, since R_r is smaller than R. Only a small amount of the variance of fU is found to be associated with τ_W in either analysis, with the largest amount (26 %) found from regression in the 5- to 11-day band. The sign of fU in that band indicates lower-layer domination. The wind stress accounts for the greatest percentage of the total variance in the 5- to 11-day band (34 %).

TABLE 4. COEFFICIENTS b_i, WITH STANDARD ERROR e_i, FROM THE LINEAR REGRESSION OF V_t, fU, P_y, AND τ_B ON τ_W FOR THE ORIGINAL AND THE BAND-PASSED TIME SERIES FROM OREGON AND NORTHWEST AFRICA

	dependent variable	original time series $b_i \pm e_i$	> 10 days $b_i \pm e_i$	5–11 days $b_i \pm e_i$	2–6 days $b_i \pm e_i$
Oregon	V_t	0.55 ± 0.18	0.17 ± 0.23	0.80 ± 0.48	0.96 ± 0.20
	fU	-0.27 ± 0.55	-0.60 ± 0.94	-1.85 ± 0.84	-0.31 ± 0.44
	P_y	1.28 ± 0.28	1.32 ± 0.57	1.55 ± 0.31	0.76 ± 0.19
	τ_B	0.14 ± 0.04	0.27 ± 0.06	0.18 ± 0.07	0.02 ± 0.03
northwest Africa	V_t	0.20 ± 0.10	0.02 ± 0.11	0.50 ± 0.21	0.61 ± 0.18
	fU	0.25 ± 0.27	-0.22 ± 0.20	0.56 ± 0.28	0.97 ± 0.45
	τ_B	0.32 ± 0.09	0.35 ± 0.08	0.34 ± 0.18	0.06 ± 0.10

For northwest Africa, the relative sizes of the regression coefficients in figure 10 are similar to the eigenvector components from the first mode of the e.o.f. analysis (figure 8). The correspondence (including a comparison of R_r and R) is very close for periods greater than 10 days and in the 5- to 11-day band. In particular, conclusions on the relative roles of V_t and τ_B, and on R_r or R, are identical. In the 2- to 6-day band, the wind-forced component from the regression analysis includes both V_t and an upper-layer-dominated fU whereas, as mentioned in §4, in the e.o.f. analysis the wind stress variance is carried in both the first and second modes where it is associated, respectively, with fU and V_t. The fact that the wind stress explains a large percentage of the variance of the sum of terms G in the 2- to 6-day band (69 %) indicates that the non-wind-forced components of those terms $(g_i - \hat{g}_i)$ tend to balance mutually such that

$$\overline{\left[\sum_{i=1}^{N} (g_i - \hat{g}_i)\right]^2} < b_T^2 \overline{\tau_W^2}.$$

6. DISCUSSION

The decomposition of a set of estimated time-dependent terms into empirical orthogonal functions, as in §4, appears to offer a systematic approach to the problem of evaluating the mutual balance of those terms. The method seems to be promising, but the extent of its effectiveness has not been completely evaluated in this application. We mention that the primary principle that defines empirical orthogonal functions is that each mode, in succession, extract the maximum amount of variance. This feature dictates the structure of the decomposition more strongly than the constraint that the amplitudes be uncorrelated and that should be kept in mind when the results are interpreted. An idealized example, which illustrates possible problems in drawing conclusions from this type of analysis, is given below.

PHILOSOPHICAL TRANSACTIONS OF THE ROYAL SOCIETY A MATHEMATICAL, PHYSICAL & ENGINEERING SCIENCES

Assume that there are three terms V_t, P_y, τ_W and that the wind stress is composed of two uncorrelated components with equal variance, i.e. that $\tau_W = \tau_1 + \tau_2$, $\overline{\tau_1 \tau_2} = 0$, $\overline{\tau_1^2} = \overline{\tau_2^2}$. Suppose also, perhaps because of a difference in the alongshore scales of τ_1 and τ_2, that $V_t = \tau_1$ and $P_y = \tau_2$, where for simplicity noise is omitted. The empirical orthogonal function decomposition for this situation is

$$\left.\begin{aligned} V_t = aE_1 + bE_2, \quad P_y = aE_1 - bE_2, \quad \tau_W = cE_1, \\ E_1 = c^{-1}(\tau_1 + \tau_2), \quad E_2 = b(\tau_1 - \tau_2), \quad E_3 = 0, \\ \lambda_1 = \overline{3\tau_1^2}, \quad \lambda_2 = \overline{\tau_1^2}, \quad \lambda_3 = 0, \quad a = 6^{-\frac{1}{2}}, \quad b = 2^{-\frac{1}{2}}, \quad c = (\tfrac{2}{3})^{\frac{1}{2}}. \end{aligned}\right\} \tag{17}$$

The time variability of the first mode is the same as the wind stress, the sum of τ_1 and τ_2. The e.o.fs do not separate the two original uncorrelated modes of variability and, in fact, they cannot do so because of the orthogonality constraint. An examination of the above results might lead to the conclusion that the motion is composed of a wind-forced component, which is true, and a free wave component involving only V_t and P_y, which is not true. In the wind-forced component, τ_W is perfectly represented, but V_t and P_y only partially so. It is interesting that the determination here of a wind-forced component by regression analysis, as in §5, gives a result identical to the e.o.f. analysis.

The above example indicates that results from an e.o.f. decomposition of estimated terms should be interpreted with caution. Further study may show that there is a decomposition based on a different extremization principle, involving another set of uncorrelated (but not necessarily orthogonal) modes, that is more appropriate for evaluating a balance of terms.

In the application of the empirical orthogonal functions to study balances as a function of frequency, we initially considered the use of the frequency-domain e.o.fs developed by Wallace & Dickinson (1972). A straightforward application of that technique does not appear suitable, however, because terms that are highly coherent but out of phase, as V_t and τ_B frequently are, do not balance each other, but would show up in the same eigenfunction. Although a method similar to that of Wallace & Dickinson (1972) might be used to extract in-phase components, we decided to simply band-pass filter the time series and apply time domain e.o.f. analysis to the band-passed series.

A determination of the wind-forced component of the flow by regression analysis provides an objective method for evaluating the characteristics of the response to τ_W. The results from the regression analysis for Oregon and northwest Africa are qualitatively similar to those from the e.o.f. analysis when one empirical mode carries most of the wind stress variance. If the flow is not strongly wind-driven, as off Peru, then of course regression on τ_W is not very useful.

7. Summary

The salient results from the analyses in this paper may be summarized as follows. For Oregon, there is a relatively large amount of variance associated with fU which is not balanced by other estimated terms. This variability in fU might be associated with baroclinic alongshore pressure gradients or with nonlinear advection of momentum, neither of which are represented in the analysis. Otherwise, there is a substantial wind-driven component of the flow involving V_t and P_y. Bottom friction does not seem to play an important role even for periods greater than 10 days, where the balance appears to be primarily between P_y and τ_W, and where V_t has a magnitude comparable with τ_B.

PHILOSOPHICAL TRANSACTIONS OF THE ROYAL SOCIETY A MATHEMATICAL, PHYSICAL & ENGINEERING SCIENCES

Off northwest Africa, a large part of the variance of V_t and τ_B can be associated with a wind-forced component. For periods greater than 10 days, the response to τ_W appears to be quasi-steady, and bottom friction τ_B plays a dominant role. In the 5- to 11-day band, the magnitudes of V_t and τ_B in the wind-forced component are similar, which indicates comparable importance for time-dependence and frictional damping. In contrast, the response in the 2-6 day band primarily involves V_t and fU with bottom friction τ_B evidently not important.

For Peru, the motion in all the frequency bands is dominated by an inviscid, unforced balance between P_y and different combinations of V_t and fU. For periods greater than 10 days, V_t is small and fU balances P_y. In the 5- to 11-day band, where a large fraction of the variance in the alongshore velocity field is involved with poleward-propagating disturbances (Smith 1978), the balance is primarily between V_t and P_y, which is indicative of dynamics similar to that of internal Kelvin waves.

This research was supported by the National Science Foundation: for J. S. Allen by grants OCE-7826820 and OCE-8014939 and for R. L. Smith by grants OCE-7925019 and OCE-8024116. We thank Dr D. Halpern for providing wind and surface layer current measurements, G. Halliwell and W. E. Gilbert for assistance with the computations, and Dr R. E. Davis for helpful discussion.

Appendix

The wind and current data were originally sampled at intervals of 20 min or less; these data were averaged to provide hourly data sets. Hourly sea level (from tide gauges) and atmospheric pressure data were obtained from coastal stations. Hourly wind stress was computed from the hourly wind velocity, extrapolated to the 10 m level by assuming a logarithmic wind profile, by using the aerodynamic square law with a constant drag coefficient of 1.3×10^{-3} (Halpern 1976*b*). The hourly data sets were then filtered to eliminate tidal and higher frequencies by means of a symmetrical low-pass filter (half power at period of 40 h) spanning 121 h. The low-pass filtered series, resampled at 6 h intervals, were used as the basic data sets for this paper.

Not all the instruments deployed during an experiment provided identical record lengths; the sets of current meter data and the time intervals used in this paper were the largest possible within the constraints that wind velocity data were available from a nearby buoy and that a sufficiently dense vertical array of current meters was available to estimate the vertically integrated velocity.

Off Oregon, data from current meters, at 3, 8, 10, 14, 16, 18, 20, 40, 60, 80 and 95 m in 100 m of water, were used for the period 12h00 G.M.T., 6 July – 18h00 G.M.T., 26 August 1973. Wind velocity was measured from a buoy directly over the current meter moorings. Sea-level data were obtained from coastal tide stations at Newport (44° 37′ N) and the Umpqua River (43° 40′ N), both south of the current meter moorings at 45° 16′ N ($f = 1.03 \times 10^{-4}$ s^{-1}).

Off northwest Africa, data from current meters, at 1, 10, 12, 16, 25, 45, and 66 m in 73 m of water, were used for the period 00h00 G.M.T., 11 March–18h00 G.M.T., 16 April 1974. The wind velocity record was a composite of data from meteorological buoys within 16 km of the current meters which were at 21° 40′ N ($f = 0.54 \times 10^{-4}$ s^{-1}).

Off Peru, data from current meters, at 2, 5, 8, 12, 16, 20, 24, 39, 59, 80, 100 and 115 m in 121 m of water, were used for the period 18h00 G.M.T., 7 March – 06h00 G.M.T., 13 May 1977. Wind velocity was obtained from a meteorological buoy moored 8.5 km shoreward of the

current meters. Sea level was obtained at coastal tide stations at San Martin (13° 50′ S) and San Juan (15° 21′ S); the current meters were at 15° 06′ S ($f = -0.38 \times 10^{-4}$ s^{-1}).

The principal axes coordinate system (see, for example, Kundu & Allen 1976) for the depth-integrated velocity and, for comparison, the 'visual' best fit to the isobaths on bathymetric charts are specified in order by the angle of rotation, measured counterclockwise, from the geographic (east–north) coordinate system: Oregon (−1.1°, 2°), northwest Africa (3.0°, 3°), Peru (43.8°, 49°).

The statistical significance of the correlation coefficients in tables 1 and 3 is found by using integral time-scales calculated from (A 1) in Allen & Kundu (1978), which follows Davis (1976). Similarly, the standard errors of the regression coefficients in tables 3 and 4 are calculated from (A 4) in Allen & Kundu (1978).

The depth integration of the velocity components is accomplished by using the trapezoidal rule. The integral of u over an interior interval $\Delta z_{n+\frac{1}{2}} = z_{n+1} - z_n$, where z_n are the current meter locations, is approximated by

$$I_{n+\frac{1}{2}} = \int_{z_n}^{z_{n+1}} u \, \mathrm{d}z \approx \hat{I}_{n+\frac{1}{2}} = \tfrac{1}{2}\Delta z_{n+\frac{1}{2}} [u(z_{n+1}) + u(z_n)]. \tag{A1}$$

Contributions from the two boundary intervals are calculated simply by $\hat{I}_{\frac{1}{2}} = u(z_1)\,|H - z_1|$ and $\hat{I}_{N+\frac{1}{2}} = u(z_N)\,|z_N|$, where N is the total number of current meters and $z_{n+1} > z_n$.

For an exponentially varying function $u = u_0 \exp(kz)$, the relative error $E_{n+\frac{1}{2}} = |1 - (\hat{I}_{n+\frac{1}{2}}/I_{n+\frac{1}{2}})|$ of the approximation (A 1) is

$$E_{n+\frac{1}{2}} = |1 - [\tfrac{1}{2}k\Delta z_{n+\frac{1}{2}}/\tanh(\tfrac{1}{2}k\Delta z_{n+\frac{1}{2}})]|. \tag{A 2}$$

We estimate the error in the depth integrals by using (A 2) and an approximation for the value of the inverse scale length k characterizing local vertical variations. Since the vertical structure of the cross-shelf velocity u is generally more complex than that of the alongshore velocity v, we concentrate on estimating errors for the depth integration of u. With $u = u_0\, \mathrm{e}^{kz}$ and $u(z_n) = u_n$, it follows that $(u_{n+1} - u_n)/(u_{n+1} + u_n) = \tanh(\tfrac{1}{2}k\Delta z_{n+\frac{1}{2}})$. Guided by this expression, we obtain estimates of $\tfrac{1}{2}k\Delta z_{n+\frac{1}{2}}$ from

$$\tanh(\tfrac{1}{2}k\Delta z_{n+\frac{1}{2}}) = (u_{n+1} - u_n)'/(u_{n+1} + u_n)', \tag{A 3}$$

where, as before, primes indicate standard deviations. Since all nearest-neighbour correlations of u_n are positive, i.e. $\{u_{n+1}, u_n\} > 0$, the right-hand side of (A 3) is less than one for all estimates, and the assumption of an exponential variation is not inconsistent. Note, for uncorrelated components, $\{u_{n+1}, u_n\} = 0$, (A 3) implies $E_{n+\frac{1}{2}} \to \infty$.

The maximum and the average values of $E_{n+\frac{1}{2}}$ found from the low-passed data for Oregon, northwest Africa, and Peru are (0.17, 0.06), (0.56, 0.13), and (0.14, 0.06), respectively. The maximum value of $E_{n+\frac{1}{2}}$ was found for Oregon between 20 and 40 m, for northwest Africa between 25 and 45 m, and for Peru between 24 and 39 m depths. Not surprisingly, it is within these depth intervals that the mean cross-shelf flow changes sign (Smith 1981).

We assume that an estimate of the relative error for the total depth integral is

$$E_{\mathrm{T}} = \sum_{n=1}^{N-1} \tfrac{1}{2}\Delta z_{n+\frac{1}{2}} (u_{n+1} + u_n)' \, E_{n+\frac{1}{2}} \left[\sum_{n=1}^{N-1} \tfrac{1}{2}\Delta z_{n+\frac{1}{2}} (u_{n+1} + u_n)' \right]^{-1}, \tag{A 4}$$

where contributions from the two boundary intervals are omitted. For Oregon, northwest Africa, and Peru, the values of E_{T} are 0.09, 0.19, and 0.09, respectively.

References (Allen & Smith)

Allen, J. S. 1980 *A. Rev. Fluid Mech.* **12**, 389–433.
Allen, J. S. & Kundu, P. K. 1978 *J. phys. Oceanogr.* **8**, 13–27.
Badan-Dangon, A. R. F. 1981 Ph.D. dissertation (167 pp.), Oregon State University, Corvallis.
Brink, K. H., Halpern, D. & Smith, R. L. 1980 *J. geophys. Res.* **85**, 4036–4048.
Csanady, G. T. 1978 *J. phys. Oceanogr.* **8**, 47–62.
Davis, R. E. 1976 *J. phys. Oceanogr.* **6**, 249–266.
Enfield, D. B. & Allen, J. S. 1980 *J. phys. Oceanogr.* **10**, 557–578.
Halpern, D. 1976*a* *Deep-Sea Res.* **23**, 495–508.
Halpern, D. 1976*b* *J. phys. Oceanogr.* **6**, 108–112.
Halpern, D., Smith, R. L., & Mittelstaedt, E. 1977 *J. mar. Res.* **35**, 787–796.
Huyer, A. 1976 *J. mar. Res.* **34**, 531–546.
Kundu, P. K., Allen, J. S. & Smith, R. L. 1975 *J. phys. Oceanogr.* **5**, 683–704.
Kundu, P. K. & Allen, J. S. 1976 *J. phys. Oceanogr.* **6**, 181–199.
Smith, R. L. 1974 *J. geophys. Res.* **79**, 435–443.
Smith, R. L. 1978 *J. geophys. Res.* **83**, 6083–6092.
Smith, R. L. 1981 In *Coastal upwelling research*, 1980 (ed. F. A. Richards). Washington, D.C.: American Geophysical Union.
Wallace, J. M. & Dickinson, R. E. 1972 *J. appl. Meteorol.* **11**, 887–892.

PHILOSOPHICAL TRANSACTIONS OF THE ROYAL SOCIETY A MATHEMATICAL, PHYSICAL & ENGINEERING SCIENCES